Gopalarathnam and Kumar *International Journal of Advanced Structural Engineering* 2013, 5:27
http://www.advancedstructeng.com/content/5/1/27

International Journal of Advanced Structural Engineering
a SpringerOpen Journal

ORIGINAL RESEARCH Open Access

Nonlinear finite element dynamic analysis of squat shear wall with openings

Muthukumar Gopalarathnam* and Manoj Kumar

Abstract

Shear wall has been considered as a major lateral load-resisting element in multistoried building located in wind- or earthquake-prone zone. The behavior of shear wall under various loading conditions has been the subject of intense research for the last few decades. The behavior of shear walls without openings is completely well understood and well documented in literature. The use of squat shear wall has been found in many low-rise buildings. On the other hand, squat shear walls may also be provided with openings due to the functional requirement such as placement of doors/windows in the building. The size and location of the opening play a significant role in the response of the shear wall. Even though it is intuitively known that the size of opening has significant effects on the behavior of a shear wall, it is desirable to know the limiting size of opening in the shear wall, beyond which the shear walls may fail or become unserviceable, especially when subjected to severe earthquake ground motions. In this study, the materially nonlinear dynamic response of the shear wall, with and without openings for different damping ratios, subjected to EL Centro earthquake has been captured. For dynamic analysis, constant acceleration Newmark β method of direct time integration has been used. From the study, it was observed that the presence of opening results in severe displacements and stresses on the shear wall and also results in stress concentration near the opening tip. Hence, the presence of damping has been considered to be vital for large opening under severe dynamic loading conditions.

Keywords: Squat; Shear wall; Openings; Structural response; Nonlinear; Dynamic; Newmark; Damping; Cracking

Introduction

The reinforced concrete tall buildings are subjected to lateral loads such as wind and earthquake. In order to resist the lateral load, shear walls are provided in the framed structures as a lateral load resisting element (Rahimian 2011, Kim and Lee 2008, Kuang and Ho 2008). The importance of shear wall in mitigating the damage to reinforced concrete structures is well documented in the literature (Kuang and Ho 2008). The reinforced concrete and masonry shear walls have been in use for many decades as a major structural configuration to resist wind and earthquake forces. In general, masonry shear walls are modeled using no-tension assumption given the fact that masonry hardly resists tensile forces (Corbi 2013; Baratta and Corbi 2010). The assumption of no-tension results in the tremendous reduction in the computational effort in masonry structures (Baratta et al. 2008, Baratta and Corbi 2010; Baratta and Corbi 2012). The shear wall should possess sufficient strength and stiffness under any loading conditions. The shear walls are generally classified on the basis of aspect ratio (height/width ratio). The shear walls with aspect ratio between 1 and 3 are generally considered to be of squat type and shear walls with aspect ratio greater than 3 are considered to be of slender type. In general, the structural response of shear wall depends strongly on the type of loading, aspect ratio of shear wall, size, and location of the openings in the shear wall. The squat shear walls generally fail in racking/shear mode whereas the slender shear walls fail in a flexural mode. In the case of low-rise shear walls, the racking deformation, a kind of shear deformation, becomes predominant and substantially contributes to the overall deformation. The squat shear walls are frequently used in low-rise multistoried buildings as well as in high-rise buildings where the shear walls are extended up to few stories only. The importance of overturning of rigid blocks and racking deformation was described by Baratta

* Correspondence: muthug@pilani.bits-pilani.ac.in
Department of Civil Engineering, BITS, Pilani 333031, India

et al. (2012, 2013), as squat shear walls are more vulnerable to overturning. Various experimental and analytical studies have been performed to investigate the response of solid shear wall under monotonic loading conditions (Lefas et al. 1990; Derecho et al. 1979; Mullapudi et al. 2009; Paknahad et al. 2007). Sometimes openings are provided in the shear wall due to functional requirements. The structural behavior of the shear wall with opening becomes complex due to the stress concentration near the openings (Neuenhofer 2006). Many experimental investigations have been performed on reinforced concrete shear walls with and without openings subjected to severe dynamic earthquake loading conditions (Mo 1988; Ricci et al. 2012; Gasparani et al. 2013). The aspect ratio of shear wall plays a significant role on the structural response of shear wall with openings. The elastic analysis of shear wall can be performed using (a) continuous connection method (CCM), (b) transfer matrix method, (c) wide column analogy (WCA) or frame analysis, (d) finite element method, and (e) discrete force method. Neuenhofer (2006) has observed that for the same opening area, the reduction in stiffness for squat and slender shear walls are 50% and 20%, respectively. Thus, the aspect ratio becomes critical for squat shear walls. Few analytical studies have been made on the response of shear wall with openings (Neuenhofer 2006; MacLeod 1970; Rosman 1964; Schwaighofer 1967; Taylor et al. 1988). Rosman (1964) developed an approximate linear elastic approach using laminar analysis, based on different assumptions to analyze the shear wall with one row and two rows of openings. Schwaighofer (1967) used this approach to analyze the shear wall with three rows of openings and observed that the Rosman's theory predicts the behavior of shear wall with three rows of openings also with sufficient accuracy. Conventional methods such as CCM, transfer matrix method, and WCA cannot be used to analyze the complex structure such as shear walls with openings. Moreover, it was found that the conventional methods result in remarkably poor results for the squat shear walls where the mode of failure is predominantly shear. It was also shown in literature that the hand calculation either underestimates/overestimates the response in predicting the response of shear wall with openings (Neuenhofer 2006). In order to make realistic predictions of strength, stiffness, and seismic energy dissipation capacity, it is essential to use proper numerical technique. The finite element analysis has been the most versatile and successfully employed method of analysis in the past to accurately predict the structural behavior of reinforced concrete shear wall in linear as well as nonlinear range under any severe loading conditions. With the advent in computing facilities, finite element method has gained an enormous popularity among the structural engineering community, especially in the nonlinear dynamic analysis. The nonlinearity of the structure may be due to the geometry or material. Since shear wall is a huge structure, the deformation of the shear wall was assumed to be in control and hence, the geometric nonlinearity has not been considered. In the present study, the two-dimensional analysis of the shear wall using finite element methods has been conducted in order to accurately predict the modes of failure. In this study, nonlinear dynamic finite element two-dimensional analysis of reinforced concrete shear wall with and without openings has been carried out using nine-node degenerated shell element with five degrees of freedoms at each node.

In order to investigate the influence of opening sizes on the elastic response of squat shear wall, a shear wall with dimensions of 3.6 m high, 3.6 m wide and 0.2-m-thick shear wall, subjected to EL Centro earthquake loading acting over the period of 31.18 s, has been considered. The total earthquake loading spreading over 31.18 s has been discretized into an interval of 0.02 s, thus resulting in 1,558 data points. The concentrated mass of 1,000 kN is located at the top of the shear wall. Nevertheless, in order to investigate the post-earthquake effect on shear wall, the displacement response of shear wall has been captured until 40 s. Since every structure possesses some inherent damping, a minimum damping ratio of 2.5% has been considered. The Rayleigh damping has been employed with stiffness proportionality only to a circular frequency of 10 rad/second. In order to investigate the size of opening on structural response of shear wall, three different sizes of openings are considered, namely, (a) small opening (1.2 m × 1.2 m), (b) medium opening (1.2 m × 2.4 m), and (c) large opening (2.4 m × 2.4 m). Newmark β method of direct time integration with constant acceleration scheme, consistent mass matrix, and Rayleigh damping, have been adopted to calculate the dynamic response at discrete time intervals. The analysis has also been carried out for different ratios 5%, 7.5%, and 10%. The results of the shear wall with openings are compared with the solid shear wall.

Methods

Geometric modeling

The displacement-based finite element method has been considered to be the most popular choice because of its simplicity and ease with which the computations can be performed. The use of shell element to model moderately thick structures like shear wall is well documented in the literature (Liu and Teng 2008). Nevertheless, the general shell theory based on the classical approach has been found to be complex in the finite element formulation. On the other hand, the degenerated shell element (Ahmad et al. 1970, Kant et al. 1994) derived from the

three-dimensional element has been quite successful in modeling moderately thick structures because of their simplicity and has circumvented the use of classical shell theory. The degenerated shell element (Figure 1) is based on the assumption that the normal to the middle surface remains straight but not necessarily normal after deformation. Also, the stresses normal to the middle surface are considered to be negligible. However, when the thickness of element reduces, the degenerated shell element has suffered from shear locking and membrane locking when subjected to full numerical integration. The shear locking and membrane locking are the parasitic shear stresses and membrane stresses present in the finite element solution. In order to alleviate locking problems, the reduced integration technique has been suggested and adopted by many authors (Zienkiewicz et al. 1971; Paswey and Clough 1971). However, the use of reduced integration resulted in spurious mechanisms or zero energy modes in some cases. The reduced integration ignores the high-ranked terms in interpolated shear strain by numerical integration, thus introducing the chance of development of spurious or zero energy modes in the element. The selective integration, wherein different integration orders are used to integrate the bending, shear, and membrane terms of stiffness matrix, avoids the locking in most of the cases. The assumed strain approach has been successfully adopted by many researchers (Huang 1989; Bathe 2006) as an alternative to avoid locking. In the assumed strain-based degenerated shell elements, the transverse shear strain and membrane strains are interpolated from the assumed sampling points (Figure 2) obtained from the compatibility requirement between flexural and shear strain fields respectively.

Thus, the assumed strain approach allows the use of full integration, avoiding the risk of zero energy modes. In this element, five degrees of freedom are considered at each node, comprising three translations and two

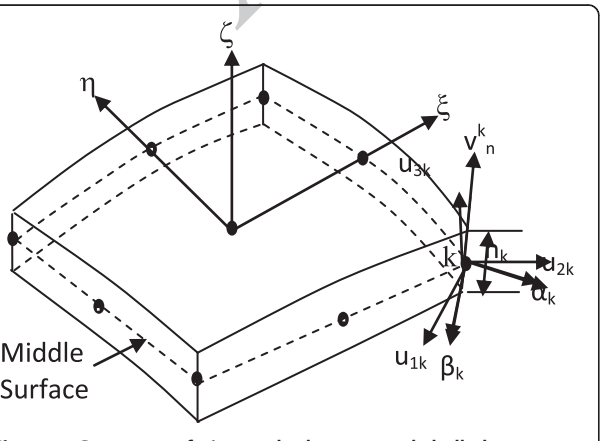

Figure 1 Geometry of nine-node degenerated shell element.

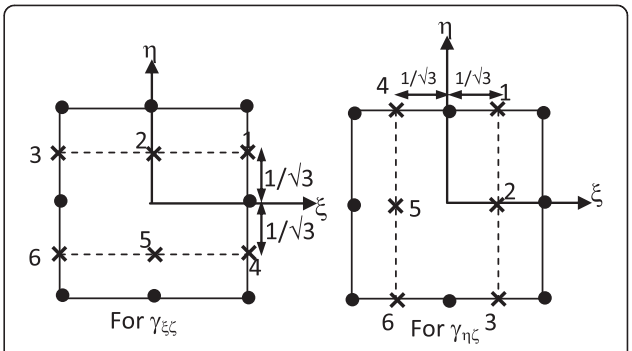

Figure 2 Sampling point locations for assumed shear/membrane strains.

rotations of the normal. The formulation of degenerated isoparametric shell element is completely described by Huang (1989). The geometry of the degenerated shell element can be conveniently represented by the coordinates and normal vectors of the middle surface. In general, the geometry and kinematics of deformations are described by using different coordinate systems. The Cartesian coordinate system is used to define the geometry of the structure, nodal coordinates and displacements, global stiffness matrix, and applied load vector. The coordinates of a point within an element are obtained by interpolating the nodal coordinates through the element shape functions:

$$\begin{Bmatrix} x \\ y \\ z \end{Bmatrix} = \sum_{k=1}^{9} N_k(\xi,\eta) \begin{Bmatrix} x_k \\ y_k \\ z_k \end{Bmatrix}_{\text{mid}} + \sum_{k=1}^{9} N_k(\xi,\eta) \frac{\zeta\, h_k}{2} \begin{Bmatrix} V_{3k}^x \\ V_{3k}^y \\ V_{3k}^z \end{Bmatrix}. \tag{1}$$

The displacements at any point inside the finite element can also be expressed by

$$\begin{Bmatrix} u \\ v \\ w \end{Bmatrix} = \sum_{k=1}^{n} N_k \begin{Bmatrix} u_k \\ v_k \\ w_k \end{Bmatrix}_{\text{mid}} + \sum_{k=1}^{n} N_k \zeta \frac{h_k}{2} \begin{bmatrix} v_{1k}^x & -v_{2k}^x \\ v_{1k}^y & -v_{2k}^y \\ v_{1k}^z & -v_{2k}^z \end{bmatrix} \begin{bmatrix} \beta_{1k} \\ \beta_{2k} \end{bmatrix} \tag{2}$$

In the above expression, $N_k(\xi,\eta)$ are the element shape functions and h_k is the shell thickness at node k. V_{ik} are the natural coordinates at any node k under consideration. A nodal coordinate system is defined at each nodal point with origin situated at the reference mid-surface. The vector $\mathbf{V}_{3k}$ is constructed from the nodal coordinates at top and bottom surfaces and is expressed as

$$\mathbf{v}_{3k} = \begin{Bmatrix} x_k \\ y_k \\ z_k \end{Bmatrix}_{top} - \begin{Bmatrix} x_k \\ y_k \\ z_k \end{Bmatrix}_{bottom}. \tag{3}$$

v_{3k} defines the direction of the normal at any node 'k', which is not necessarily perpendicular to the mid-surface. The major advantage of the definition of v_{3k}

with normal but not necessarily perpendicular to mid-surface is that there are no gaps or overlaps along element boundaries. The element shape functions are calculated in the natural coordinate system as

$$\left.\begin{aligned}
N_1 &= \frac{1}{4}\xi(1+\xi)\eta(1+\eta)\\
N_2 &= \frac{1}{2}(1+\xi)(1-\xi)\eta(1+\eta)\\
N_3 &= -\frac{1}{4}(1-\xi)\eta(1+\eta)\\
N_4 &= -\frac{1}{2}\xi(1-\xi)(1+\eta)(1-\eta)\\
N_5 &= \frac{1}{4}(1-\xi)\eta(1-\eta)\\
N_6 &= -\frac{1}{2}(1+\xi)(1-\xi)\eta(1-\eta)\\
N_7 &= -\frac{1}{4}\xi(1+\xi)\eta(1-\eta)\\
N_8 &= \frac{1}{2}\xi(1+\xi)(1+\eta)(1-\eta)\\
N_9 &= (1+\xi)(1-\xi)(1+\eta)(1-\eta)
\end{aligned}\right\}. \tag{4}$$

Once the displacements are determined, the strains and stresses are calculated using strain–displacement matrix and material constitutive matrix, respectively. Since the resultant stresses in the z-direction (out-of-plane direction) are considered to be 0, there are only five independent strains. The strain condition at a point is defined by the vector

$$\varepsilon = \left[\varepsilon_x\ \varepsilon_y\ \gamma_{xy}\ \gamma_{xz}\ \gamma_{yz}\right]. \tag{5}$$

Since geometric nonlinearity is not considered, the five strain components are related to displacements of only first order:

$$\boldsymbol{\varepsilon} = \begin{bmatrix} \varepsilon_{x'} \\ \varepsilon_{y'} \\ \gamma_{x'y'} \\ \gamma_{x'z'} \\ \gamma_{y'z'} \end{bmatrix} = \begin{bmatrix} \dfrac{\partial u'}{\partial x'} \\ \dfrac{\partial v'}{\partial y'} \\ \dfrac{\partial u'}{\partial y'} + \dfrac{\partial v'}{\partial x'} \\ \dfrac{\partial u'}{\partial z'} + \dfrac{\partial w'}{\partial x'} \\ \dfrac{\partial v'}{\partial z'} + \dfrac{\partial w'}{\partial y'} \end{bmatrix}. \tag{6}$$

The transformation matrix has been used to convert the local coordinate system into global coordinate system.

$$\begin{bmatrix} \dfrac{\partial u'}{\partial x'} & \dfrac{\partial v'}{\partial x'} & \dfrac{\partial w'}{\partial x'} \\ \dfrac{\partial u'}{\partial y'} & \dfrac{\partial v'}{\partial y'} & \dfrac{\partial w'}{\partial y'} \\ \dfrac{\partial u'}{\partial z'} & \dfrac{\partial v'}{\partial z'} & \dfrac{\partial w'}{\partial z'} \end{bmatrix} = [\mathbf{T}]^T \begin{bmatrix} \dfrac{\partial u}{\partial x} & \dfrac{\partial v}{\partial x} & \dfrac{\partial w}{\partial x} \\ \dfrac{\partial u}{\partial y} & \dfrac{\partial v}{\partial y} & \dfrac{\partial w}{\partial y} \\ \dfrac{\partial u}{\partial z} & \dfrac{\partial v}{\partial z} & \dfrac{\partial w}{\partial z} \end{bmatrix} [\mathbf{T}] \tag{7}$$

In order to transform the Cartesian coordinate system into natural coordinate system, the Jacobian matrix has been employed:

$$\begin{bmatrix} \dfrac{\partial u}{\partial x} & \dfrac{\partial v}{\partial x} & \dfrac{\partial w}{\partial x} \\ \dfrac{\partial u}{\partial y} & \dfrac{\partial v}{\partial y} & \dfrac{\partial w}{\partial y} \\ \dfrac{\partial u}{\partial z} & \dfrac{\partial v}{\partial z} & \dfrac{\partial w}{\partial z} \end{bmatrix} = J^{-1} \begin{bmatrix} \dfrac{\partial u}{\partial \xi} & \dfrac{\partial v}{\partial \xi} & \dfrac{\partial w}{\partial \xi} \\ \dfrac{\partial u}{\partial \eta} & \dfrac{\partial v}{\partial \eta} & \dfrac{\partial w}{\partial \eta} \\ \dfrac{\partial u}{\partial \zeta} & \dfrac{\partial v}{\partial \zeta} & \dfrac{\partial w}{\partial \zeta} \end{bmatrix}, \tag{8}$$

where

$$J = \begin{bmatrix} \dfrac{\partial x}{\partial \xi} & \dfrac{\partial y}{\partial \xi} & \dfrac{\partial z}{\partial \xi} \\ \dfrac{\partial x}{\partial \eta} & \dfrac{\partial y}{\partial \eta} & \dfrac{\partial z}{\partial \eta} \\ \dfrac{\partial x}{\partial \varsigma} & \dfrac{\partial y}{\partial \varsigma} & \dfrac{\partial z}{\partial \varsigma} \end{bmatrix}. \tag{9}$$

The strain–displacement matrix [B] relates the strain and displacement components as

$$\varepsilon = \mathbf{B}\,\delta \tag{10}$$

$$\{\delta\} = [u\ v\ w\ \alpha\ \beta]^T. \tag{11}$$

The numerical integration has to be resorted to in order to evaluate the element stiffness matrix for an isoparametric degenerated shell element

$$\iint dx\,dy = \int_{-1}^{+1}\int_{-1}^{+1} \det|J|\,d\xi\,d\eta. \tag{12}$$

The layered element formulation (Teng et al. 2005) allows the integration through the element thickness, which is divided into several concrete and steel layers. Each layer is assumed to have one integration point at its mid-surface. The steel layers are used to model the in-plane reinforcement only. The assumed transverse shear strain fields, interpolated at the six appropriately located sampling points, as shown in Figure 2, are

$$\left.\begin{aligned}
\bar{\gamma}_{\xi\zeta} &= \sum_{i=1}^{3}\sum_{j=1}^{2} P_i(\eta)\,Q_j(\xi)\,\gamma_{\xi\zeta}^{ij}\\
\bar{\gamma}_{\eta\zeta} &= \sum_{i=1}^{3}\sum_{j=1}^{2} P_i(\xi)\,Q_j(\eta)\,\gamma_{\eta\varsigma}^{ij}
\end{aligned}\right\}. \tag{13}$$

In the above equation, $\gamma_{\xi\varsigma}^{ij}$ and $\gamma_{\eta\zeta}^{ij}$ are the shear strains obtained from Lagrangian shape functions.

The interpolating functions $P_i(z)$ and $Q_j(z)$ are

$$P_1(z) = \frac{z}{2}.(z+1), P_2(z) = 1-z^2, P_3(z) = \frac{z}{2}.(z-1)$$
$$Q_1(z) = \frac{1}{2}\left(1+\sqrt{3}.z\right),\ Q_2(z) = \frac{1}{2}\left(1-\sqrt{3}.z\right). \tag{14}$$

Hence, it can be observed that $\bar{\gamma}_{\xi\zeta}$ is linear in ξ direction and quadratic in η direction, while $\bar{\gamma}_{\eta\zeta}$ is linear in η direction and quadratic in ξ direction. The polynomial terms for curvature of nine-node Lagrangian element, κ_ξ and κ_η, are the same as the assumed shear strain as given by

$$\kappa_\xi = \frac{\partial\theta_\xi\left(1,\xi,\eta,\xi\eta,\xi^2,\xi^2\eta,\eta^2,\xi\eta^2,\xi^2\eta^2\right)}{\partial\xi}$$
$$\kappa_\xi = \kappa_\xi\left(1,\xi,\eta,\xi\eta,\eta^2,\xi\eta^2\right) \tag{15}$$

$$\kappa_\eta = \frac{\partial\theta_\eta\left(1,\xi,\eta,\xi\eta,\xi^2,\xi^2\eta,\eta^2,\xi\eta^2,\xi^2\eta^2\right)}{\partial\eta}$$
$$\kappa_\eta = \left(1,\xi,\eta,\xi\eta,\xi^2,\xi^2\eta^2\right) \tag{16}$$

$$\bar{\gamma}_{\xi\zeta} = \bar{\gamma}_{\xi\zeta}\left(1,\xi,\eta,\xi\eta,\eta^2,\xi\eta^2\right)$$
$$\bar{\gamma}_{\eta\zeta} = \bar{\gamma}_{\eta\zeta}\left(1,\xi,\eta,\xi\eta,\eta^2,\xi\eta^2\right). \tag{17}$$

The original shear strain obtained from the Lagrange shape functions $\gamma_{\xi\zeta}$ and $\gamma_{\eta\zeta}$ is

$$\gamma_{\xi\zeta} = \theta_\xi + \frac{\partial w}{\partial\xi} = \gamma_{\xi\zeta}\left(1,\xi,\eta,\xi\eta,\xi^2,\xi^2\eta,\eta^2,\xi\eta^2,\xi^2\eta^2\right)$$
$$\gamma_{\eta\zeta} = \theta_\eta + \frac{\partial w}{\partial\eta} = \gamma_{\eta\zeta}\left(1,\xi,\eta,\xi\eta,\xi^2,\xi^2\eta,\eta^2,\xi\eta^2,\xi^2\eta^2\right). \tag{18}$$

In the above equation, θ_ξ and θ_η are the rotating normal and w is the transverse displacement of the element. It can be clearly seen that the original shear strain and assumed shear strain are not compatible and hence the shear locking exists for very thin shell cases. The appropriately chosen polynomial terms and sampling points ensure the elimination of risk of spurious zero energy modes. The assumed strain can be considered as a special case of integration scheme wherein for function $\bar{\gamma}_{\xi\zeta}$, full integration is employed in η direction and reduced integration is employed in ξ direction. On the other hand, for function $\bar{\gamma}_{\eta\zeta}$, reduced integration is employed in η direction and full integration is employed in ξ direction. The membrane and shear strains are interpolated from identical sampling points, even though the membrane strains are expressed in orthogonal curvilinear coordinate system and transverse shear strains are expressed in natural coordinate system. The next section briefly deals with the material modeling of concrete and reinforcing steel.

Material modeling

The modeling of material play may a crucial role in achieving the correct response. The presence of nonlinearity may add another dimension of complexity to it. Many material models have been developed in the past over the years such as compression field theory (CFT) proposed by Collins and Mitchell (1980) and modified compression field theory (MCFT) proposed by Vecchio and Collins (1986) to model the cracked response of concrete in compression. The nonlinearities in the structure may accurately be estimated and incorporated in the solution algorithm. The accuracy of the solution algorithm depends strongly on the prediction of second-order effects that cause nonlinearities, such as tension stiffening, compression softening, and stress transfer nonlinearities around cracks. These nonlinearities are usually incorporated in the constitutive modeling of the reinforced concrete. In order to incorporate geometric nonlinearity, the second-order terms of strains are included. In this study, only material nonlinearity has been considered. The subsequent sections describe the modeling of concrete in compression and tension, and modeling of steel briefly.

Concrete modeling in tension

The presence of crack in concrete has much influence on the response of nonlinear behavior of reinforced concrete structures. The crack in the concrete is assumed to occur when the tensile stress exceeds the tensile strength. The cracking of concrete results in the loss of continuity in the load transfer and, hence, the stresses in both concrete as well as steel reinforcement differ significantly. Therefore, the analysis of concrete fracture has been very important in order to predict the response of structure precisely. The numerical simulation of concrete fracture can be represented either by discrete crack proposed by Ngo and Scordelis (1967) or by smeared crack proposed by Rashid (1968). The objective of discrete crack is to simulate the initiation and propagation of dominant cracks present in the structure. In the case of discrete crack approach, nodes are disassociated due to the presence of cracks and therefore, the structure requires frequent renumbering of nodes, which may render huge computational cost. Nevertheless, when the structure's behavior has been dominated by only few dominant cracks, the discrete modeling of cracking seems the only choice. On the other hand, the smeared crack approach smears out the cracks over the continuum, captures the deterioration process through the

constitutive relationship, and reduces the computational cost and time drastically.

Crack modeling has gone through several stages due to the advancement in technology and computing facilities. Earlier research work indicates that the formation of crack results in the complete reduction in stresses in perpendicular direction thus neglecting the phenomenon called tension stiffening. With the rapid increase in extensive experimental investigations as well as computing facilities, many finite element codes have been developed for the nonlinear finite element analysis, which incorporate the tension stiffening effect. The first tension stiffening model using degraded concrete modulus was proposed by Scanlon and Murray and subsequently, many analytical models have been developed such as Lin and Scordelis model, Vebo and Ghali model, and Gilbert and Warner model (Nayal and Rasheed 2006). The cracks are always assumed to be formed in the direction which is perpendicular to the direction of the maximum principal stress. These directions may not necessarily remain the same throughout the analysis and loading; hence, the modeling of orientation of crack plays a significant role on the response of the structure. Still, due to simplicity, many investigations have been performed using fixed crack approach, wherein the direction of principal strain axes may remain fixed throughout the analysis. In this study also, the direction of crack has been considered to be fixed throughout the duration of the analysis. However, the modeling of aggregate interlock has not been taken very seriously. The constant shear retention factor or the simple function has been employed to model the shear transfer across the cracks. Apart from the initiation of crack, the propagation of crack also plays a crucial role in the response of structure. The prediction of crack propagation is a very difficult phenomenon due to scarcity and conflict of test results. Nevertheless, the propagation of cracks plays a crucial role on the response of nonlinear analysis of reinforced concrete structures. The plain concrete exhibits softening behavior and reinforced concrete exhibits stiffening behavior due to the presence of active reinforcing steel. A gradual release of the concrete stress (Figure 3) is adopted in this present study (Owen and Hinton 1980).

The reduction in the stress is given by the following expression:

$$E_i = \alpha f'_t \left(1 - \frac{\varepsilon_i}{\varepsilon_m}\right) \frac{1}{\varepsilon_i}; \quad \varepsilon_t \le \varepsilon_i \le \varepsilon_m. \tag{19}$$

In the above equation, α and ε_m are the tension stiffening parameters. ε_m is the maximum value reached by the tensile strain at the point considered; ε_i is the current tensile strain in material direction 1. The coefficient α depends on the percentage of steel in the section. In the present study, the values of α and ε_m are taken as 0.5 and 0.0020, respectively. It has also been reported that the influence of the tension stiffening constants on the response of the structures is generally small and hence the constant value is justified in the analysis (Owen and Hinton 1980). Generally, the cracked concrete can transfer shear forces through dowel action and aggregate interlock. The magnitude of shear moduli has been considerably affected because of extensive cracking in different directions (Table 1).

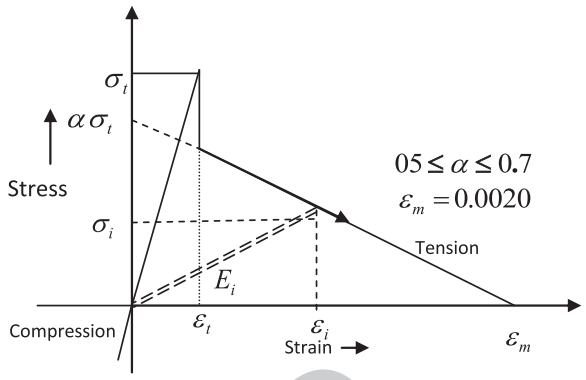

Figure 3 Tension stiffening of concrete.

Thus, the reduced shear moduli can be put to incorporate the aggregate interlock and dowel action. In the plain concrete, aggregate interlock is the major shear transfer mechanism, and for reinforced concrete, dowel action is the major shear transfer mechanism, with reinforcement ratio being the critical variable. In order to incorporate the aggregate interlock and dowel action, the appropriate value of cracked shear modulus (Cedolin et al. 1977) has been considered in the material modeling of concrete.

Concrete modeling in compression

The theory of plasticity has been used in the compression modeling of the concrete. The failure surface or bounding surface has been defined to demarcate plastic behavior from the elastic behavior. Failure surface is the important component in the concrete plasticity. Sometimes the failure surface can be referred to as yield surface or loading surface. The material behaves in an elastic fashion as long as the stress lies below the failure surface. Several failure models have been developed and reported in the literature (Chen 1982). Nevertheless, the five-parameter failure model proposed by Willam and Warnke (1975) seems to possess all inherent properties of the failure surface. The failure surface (Figure 4) is constructed using two meridians namely, compression meridian and tension meridian. The two meridians are pictorially depicted in a meridian plane

Table 1 Crack formulation

	Crack in I direction	Crack in II direction
Matrix	$\begin{bmatrix}\sigma_1\\ \sigma_2\\ \tau_{12}\\ \tau_{13}\\ \tau_{23}\end{bmatrix} = \begin{bmatrix}0&0&0&0&0\\ 0&E&0&0&0\\ 0&0&G^c_{12}&0&0\\ 0&0&0&G^c_{13}&0\\ 0&0&0&0&5G/6\end{bmatrix}\begin{bmatrix}\varepsilon_1\\ \varepsilon_2\\ \gamma_{12}\\ \gamma_{13}\\ \gamma_{23}\end{bmatrix}$	$\begin{bmatrix}\sigma_1\\ \sigma_2\\ \tau_{12}\\ \tau_{13}\\ \tau_{23}\end{bmatrix} = \begin{bmatrix}0&0&0&0&0\\ 0&0&0&0&0\\ 0&0&G^c_{12}/2&0&0\\ 0&0&0&G^c_{13}&0\\ 0&0&0&0&G^c_{23}\end{bmatrix}\begin{bmatrix}\varepsilon_1\\ \varepsilon_2\\ \gamma_{12}\\ \gamma_{13}\\ \gamma_{23}\end{bmatrix}$
Equation	$G^c_{12} = 0.25 \times G\left(1-\frac{1}{0.004}\right)$ $G^c_{12} = 0$ if $\varepsilon_1 \geq 0.004$ $G^c_{13} = G^c_{12}; G_{23} = \frac{5G}{6}$	$G^c_{13} = 0.25 \times G\left(1-\frac{\varepsilon_1}{0.004}\right)$ $G^c_{13} = 0$ if $\varepsilon_1 \geq 0.004$ $G^c_{23} = 0.25 \times G\left(1-\frac{\varepsilon_2}{0.004}\right)$ $G^c_{23} = 0$ if $\varepsilon_2 \geq 0.004$ $G^c_{12} = 0.5 \times G^c_{13}$ or $G^c_{12} = 0.5 \times G^c_{23}$ if $G^c_{23} < G^c_{13}$

and cross section of the failure surface is represented in the deviatoric plane.

The variations of the average shear stresses τ_{mt} and τ_{mc} along tensile ($\theta = 0°$) and compressive ($\theta = 60°$) meridians are approximated by second-order parabolic expressions in terms of the average normal stresses σ_m as follows:

$$\begin{aligned}\frac{\tau_{mt}}{f'_c} &= \frac{\rho_t}{\sqrt{5}f'_c} = a_0 + a_1\left(\frac{\sigma_m}{f'_c}\right) + a_2\left(\frac{\sigma_m}{f'_c}\right)^2 \quad \theta = 0^0\\ \frac{\tau_{mc}}{f'_c} &= \frac{\rho_c}{\sqrt{5}f'_c} = b_0 + b_1\left(\frac{\sigma_m}{f'_c}\right) + b_2\left(\frac{\sigma_m}{f'_c}\right)^2 \quad \theta = 60^0\end{aligned} \tag{20}$$

These two meridians must intersect the hydrostatic axis at the same point $\sigma_m/f'_c = \bar{\xi}_0$ (corresponding to hydrostatic tension); the number of parameters need to be determined is reduced to five. The five parameters (a_0 *or* b_0, a_1, a_2, b_1, b_2) are to be determined from a set of experimental data with which the failure surface can be constructed using second-order parabolic expressions.

The failure surface is expressed as

$$f(\sigma_m, \tau_m, \theta) = \sqrt{5}\frac{\tau_m}{\rho(\sigma_m, \theta)} - 1 = 0 \tag{21}$$

$$\rho(\theta) = 2\rho_c\left(\rho_c^2 - \rho_t^2\right)\cos\theta + \rho_c\left(2\rho_t - \rho_c\right) \frac{\left[4\left(\rho_c^2 - \rho_t^2\right)\cos^2\theta + 5\rho_t^2 - 4\rho_t\rho_c\right]^{1/2}}{4\left(\rho_c^2 - \rho_t^2\right)\cos^2\theta + \left(\rho_c - 2\rho_t\right)^2}. \tag{22}$$

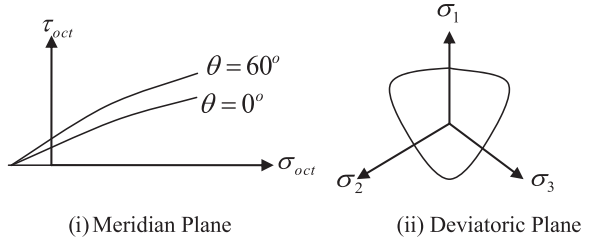

Figure 4 Failure model for concrete.

The formulation of Willam-Warnke five-parameter material model is described in Chen (1982). Once the yield surface is reached, any further increase in the loading results in plastic flow. The magnitude and direction of the plastic strain increment are defined using the flow rule which is described in the next section.

Flow rule

In this method, associated flow rule is employed because of the lack of experimental evidence in non-associated flow rule. The plastic strain increment expressed in terms of current stress increment is given as

$$d\varepsilon^p_{ij} = d\lambda\frac{\partial f(\sigma)}{\partial\sigma_{ij}}. \tag{23}$$

$d\lambda$ determines the magnitude of the plastic strain increment. The gradient $\partial f(\sigma)/\partial\sigma_{ij}$ defines the direction of plastic strain increment to be perpendicular to the yield surface; $f(\sigma)$ is the loading condition or the loading surfaces.

Hardening rule

The relationship between loading surfaces (or effective stress) and the plastic work (accumulated plastic strain) is represented by a hardening rule (Figure 5). The 'Madrid parabola' is used to define the hardening rule

$$\sigma = E_o\varepsilon - \frac{1}{2}\frac{E_0}{\varepsilon_0}\varepsilon^2. \tag{24}$$

In the above equation, E_0 is the initial elasticity modulus, ε is the total strain, and ε_0 is the total strain at peak stress f'_c. The total strain can be divided into elastic and plastic components as

$$\varepsilon = \varepsilon_e + \varepsilon_p \tag{25}$$

$$\{\dot{\sigma}\} = [D^e](\{\dot{\varepsilon}\} - \{\dot{\varepsilon}^p\}) \tag{26}$$

$$\{\dot{\varepsilon}^p\} = \dot{\lambda}\{a\} \;\; ; \quad \{a\} = \left\{\frac{\partial F}{\partial\sigma}\right\}. \tag{27}$$

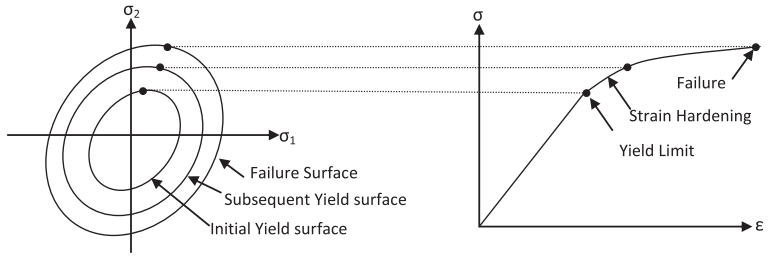

Figure 5 Isotropic hardening and the corresponding uniaxial stress–strain curve.

In the above equation, F is the yield function and $\dot{\lambda}$ is the consistency parameter which defines the magnitude of the plastic flow. The loading and unloading conditions (Kuhn-Tucker conditions) can be stated as

$$\dot{\lambda} \geq 0.; \quad F \leq 0; \quad \dot{\lambda} F = 0. \tag{28}$$

The first of these Khun-Tucker conditions indicates that the consistency parameter is non-negative; the second condition implies that the stress states must lie on or within the yield surface. The third condition ensures that the stresses lie on the yield surface during the plastic loading. The following are the conditions:

$$\begin{aligned} &\{\mathrm{a}\}^{\mathrm{T}}\{\dot{\sigma}\} = 0 \\ &\{\mathrm{a}\}^{\mathrm{T}}[\mathrm{D}^{\mathrm{e}}]\left(\{\dot{\varepsilon}\} - \{\dot{\varepsilon}_{\mathrm{p}}\}\right) = 0 \\ &\{\mathrm{a}\}^{\mathrm{T}}[\mathrm{D}^{\mathrm{e}}]\left(\{\dot{\varepsilon}\} - \dot{\lambda}\{\mathrm{a}\}\right) = 0 \\ &\dot{\lambda} = \frac{\{\mathrm{a}\}^{\mathrm{T}}[\mathrm{D}^{\mathrm{e}}]\{\dot{\varepsilon}\}}{\{\mathrm{a}\}^{\mathrm{T}}[\mathrm{D}^{\mathrm{e}}]\{\mathrm{a}\}}. \end{aligned} \tag{29}$$

The elastoplastic constitutive matrix is given by the following expression:

$$\left[D_{\mathrm{ep}}\right] = [D] - \frac{[D]\{a\}\{a\}^{T}[D]}{H + \{a\}^{T}[D]\{a\}}. \tag{30}$$

In the above equation, a = flow vector, defined by the stress gradient of the yield function; D = constitutive matrix in elastic range. The second term in the above equation represents the effect of degradation of the material during the plastic loading.

Modeling of reinforcement in tension and compression

In order to incorporate the effect of steel reinforcement, the layered approach is adopted in this study. The steel is modeled as a smeared layer of equivalent thickness in the natural coordinate system. The properties of the material are assumed to be constant in that layer. The bilinear stress–strain curve with linear elastic and strain hardening region is adopted in this study for both compression and tension. The vertical and horizontal reinforcement in the shear wall is taken as 1%; however, no ductile detailing is considered near the openings.

Table 2 Step by step Newmark β method of time integration

Step	Step description	Equation
1	Set the iteration counter	$i = 0$
2	Begin the predictor phase [displacement (d), velocity (V), acceleration (a)]	$d_{n+1}^{[i]} = d'_{n+1} + \Delta t v_{n+1} + \Delta t^2(1-2\beta)a_n/2$
		$V_{n+1}^{[i]} = v'_{n+1} = v_n + \Delta t(1-\gamma)a_n$
		$a_{n+1} = \frac{d_{n+1}^{[i]} - d'_{n+1}}{\Delta t^2 \beta} = 0$
3	Evaluation of residual forces	$\psi^{[i]} = f_{n+1} - Ma_{n+1}^{[i]} - p\left(d_{n+1}^{[i]}, v_{n+1}^{[i]}\right)$
4	Evaluation of effective stiffness matrix and solving the equation	$K^* = \frac{M}{\Delta t^2 \beta} + \frac{\gamma C_T}{\Delta t \beta} + K_T\left(d_{n+1}^{[i]}\right)$
		$K^* \Delta d^{[i]} = \psi^{[i]}$
5	Begin the corrector phase	$d_{n+1}^{[i+1]} = d_{n+1}^{[i]} + \Delta d^{[i]}$
		$v_{n+1}^{[i+1]} = v_{n+1} + \Delta t \gamma\, a_{n+1}^{[i+1]}$
		$a_{n+1}^{[i+1]} = \frac{d_{n+1}^{[i+1]} - d'_{n+1}}{\Delta t^2 \beta}$
6	Setting up the initial values for next step once the convergence is achieved	$d_{n+1} = d_{n+1}^{[i+1]};\ v_{n+1} = v_{n+1}^{[i+1]};\ a_{n+1} = a_{n+1}^{[i+1]}$

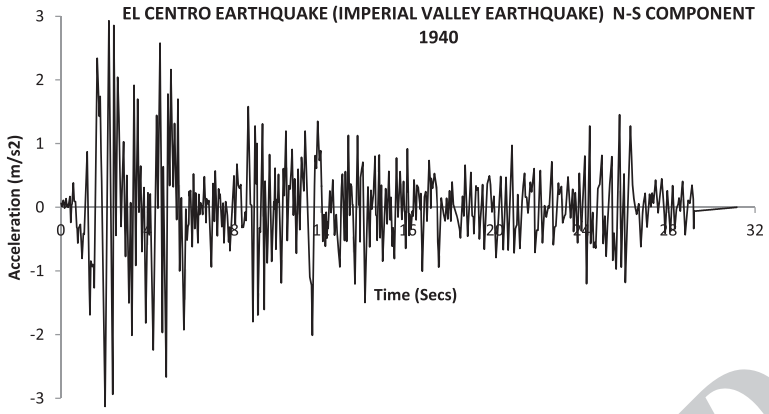

Figure 6 Acceleration time history.

Evaluation of stiffness matrix

The stiffness matrix can be calculated using the following expression

$$[K_m] = \int_0^L [B]^T [D] [B] \, dV. \tag{31}$$

Dynamic analysis

The dynamic analysis of structure can be performed by three ways, namely, (a) equivalent lateral force method, (b) response spectrum method, and (c) time-history method. The equivalent lateral force method determines the equivalent dynamic effect in a static manner. The response spectrum method aims in determining the maximum response quantity of the structure. For tall and irregular buildings, dynamic analysis by response spectrum method seems to be the popular choice among designers. The time-history analysis of the structure has been successfully used to analyze the structure especially of huge importance. Even though time-history analysis consumes time, it is the only method capable of giving results closer to the actual one especially in the nonlinear regime. In the dynamic analysis, the loads are applied over a period of time and the response is

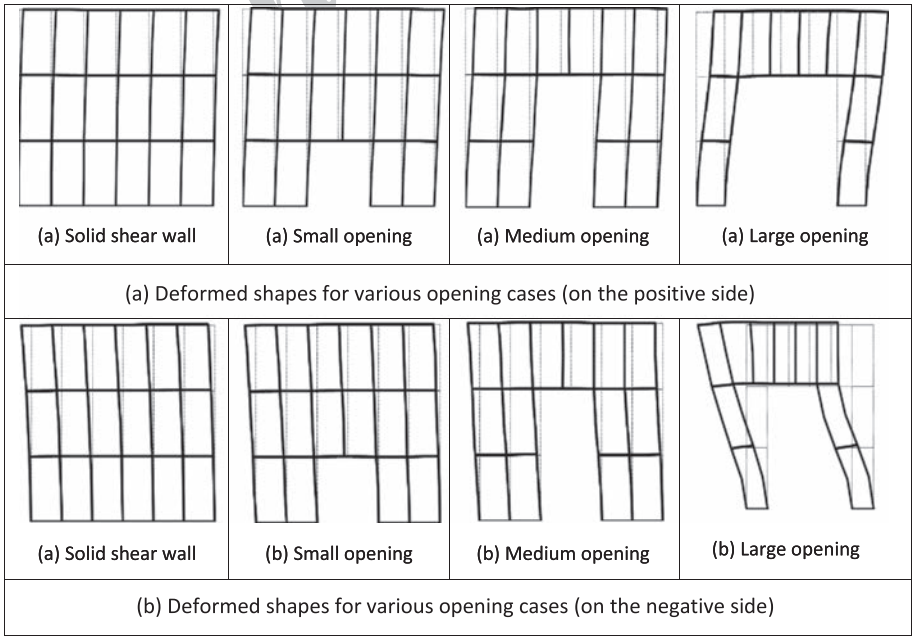

Figure 7 Undeformed and Deformed shapes of shear wall. Undeformed and Deformed shapes for various opening cases (on the positive side) and Undeformed and Deformed shapes for various opening cases (on the negative side).

obtained at different time intervals. The equation of dynamic equilibrium at any time '*t*' is given by Equation (1)

$$[M]\left[\ddot{U}^t\right] + [C]\left[\dot{U}^t\right] + [K][U^t] = [R^t]. \tag{32}$$

In the above equation, M, C and K are the mass, damping and stiffness matrices respectively. The mass matrix can be formulated either by using consistent mass approach or by using lumped mass approach. Since damping cannot be precisely determined analytically, the damping can be considered proportional to mass or stiffness or both depending on the type of the problem. The direct time integration of the equation of motion can be performed using explicit (central difference scheme) and implicit (Houbolt method, Newmark β method and Wilson Theta method, etc.) time integration. In the explicit time integration, the formation of complete stiffness matrix of the structure is not required and hence saves a lot of computer time and money in storing and saving those data. Moreover, in the case of all explicit time integration schemes, the iterations are not required as the equilibrium at time $t + \Delta t$ depends on the equilibrium at time t. Nevertheless, the major drawback of explicit time integration is that the time step (Δt) used for calculation of response has to be smaller than the critical time step (Δt_{cr}) to ensure the stable solution:

$$\Delta t \le \Delta t_{cr} = \frac{T_n}{\pi} = \frac{2}{\omega}. \tag{33}$$

On the other hand, implicit time integration requires the iterations to be carried out within the time step, as the solution at time $t + \Delta t$ involves the equilibrium equation at $t + \Delta t$. The Newmark β method converges to various implicit and explicit schemes for different values of beta, which is called the stability parameter. In this

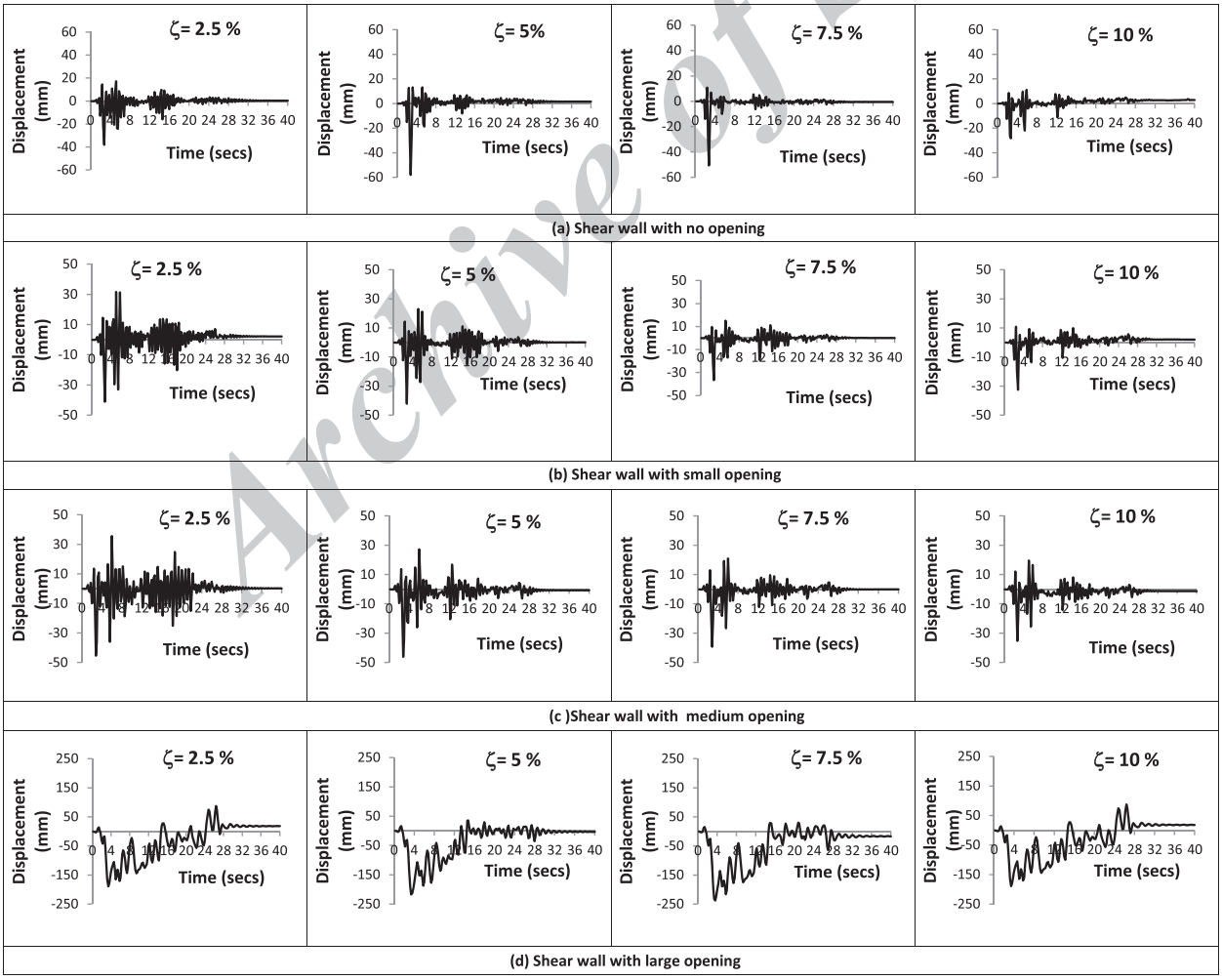

Figure 8 Top displacement time history for different damping ratios. (a) Shear wall with no opening. **(b)** Shear wall with small opening. **(c)** Shear wall with medium opening. **(d)** Shear wall with large opening.

study, for β = 0.25, the Newmark β method converges to the constant acceleration implicit method, known as trapezoidal rule. The trapezoidal rule is unconditionally stable and hence allows larger time step to be used in the calculation of response. Nevertheless, the time step can be made smaller from the accuracy point of view. The formulation of implicit Newmark β method (trapezoidal rule) is mentioned in Table 2 (Bathe 2006).

Formulation of mass matrix

In any dynamic analysis, the formulation of mass matrix is very important in capturing the correct response of a structure. The masses can be assumed to be distributed over the entire finite element mesh or can be assumed to be lumped at nodes. The former is known as consistent mass matrix and the latter is known as lumped mass matrix. The mass matrix is said to be consistent if the formulation involves the same shape functions (N_i) as used for the determination of stiffness matrix. The consistent mass matrix contains off-diagonal terms. Nevertheless, the consistent mass matrix is computationally expensive. The consistent element mass matrix is given by

$$[M_e] = \int_V \rho [N_i][N_i]^T dV. \tag{34}$$

For linear or translational motion, resistance of an object to a change of state in motion is measured in terms of mass and is given by Newton's law as follows:

$$F = ma. \tag{35}$$

On the other hand, when a rigid body is rotated, the resistance of object to a change of state in a rotating motion given by rotational inertia measured in terms of moment of inertia. The influence of rotary inertia in the case of thick plates is established in the literature

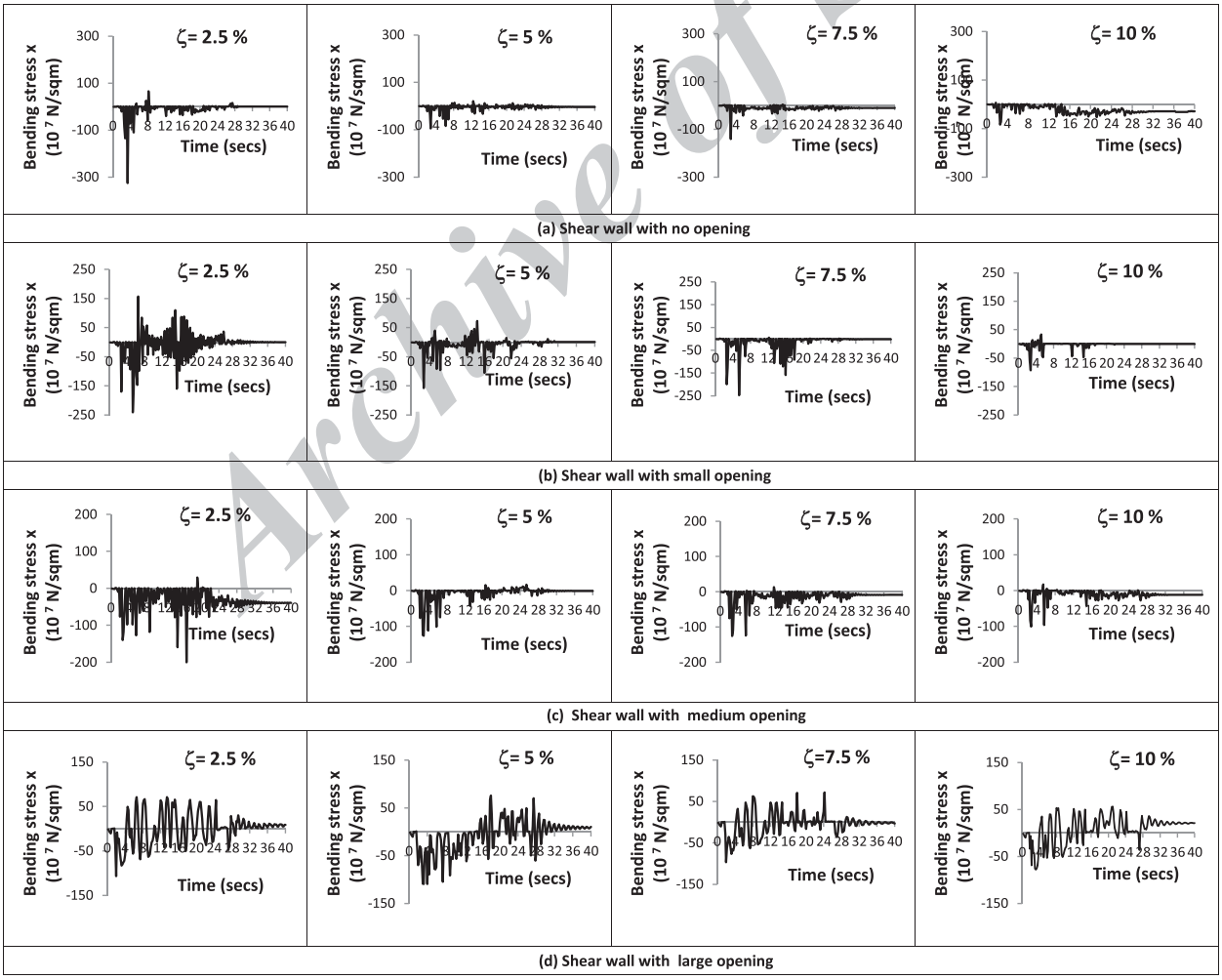

Figure 9 Top bending stress time history for different damping ratios. (a) Shear wall with no opening. **(b)** Shear wall with small opening. **(c)** Shear wall with medium opening. **(d)** Shear wall with large opening.

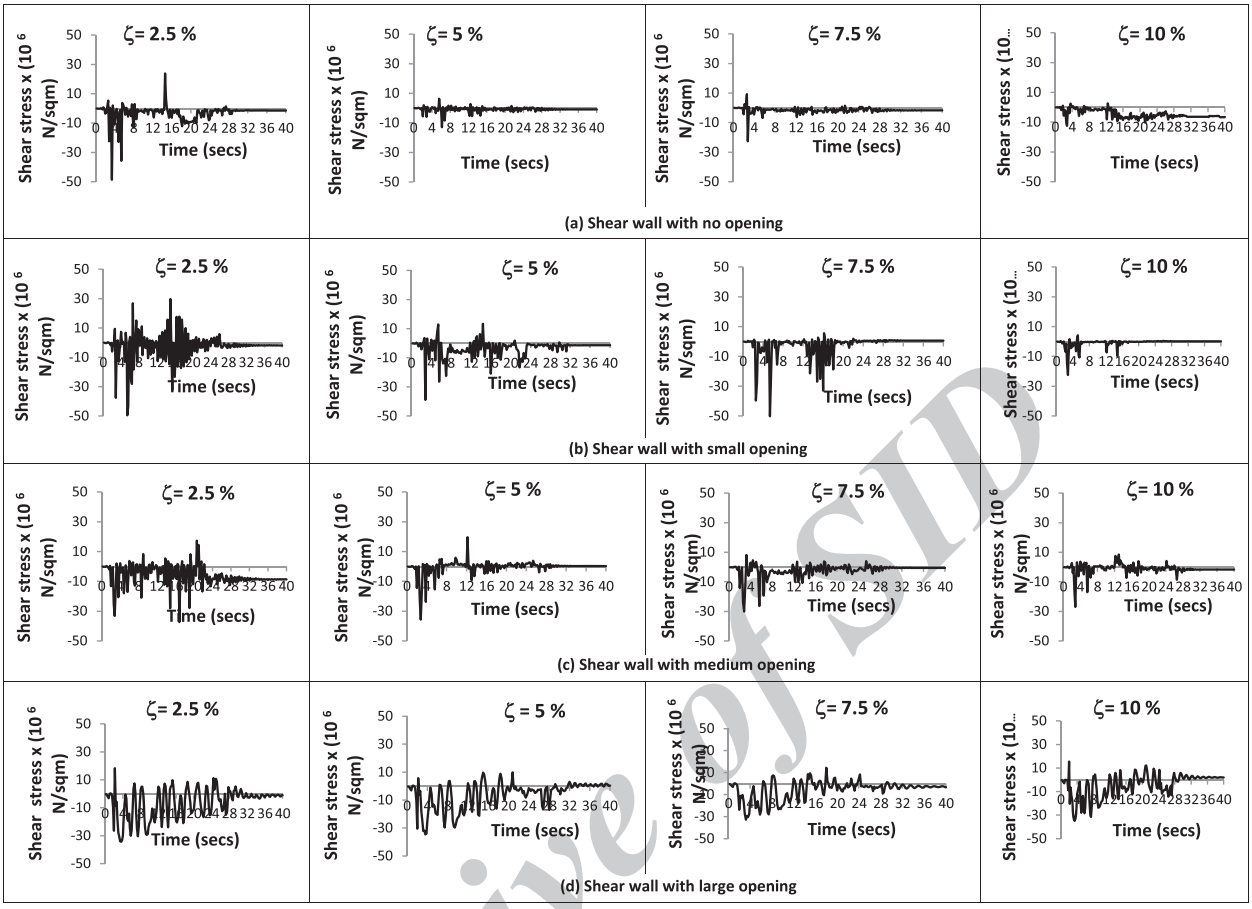

Figure 10 Top shear stress time history for different damping ratios. (a) Shear wall with no opening. **(b)** Shear wall with small opening. **(c)** Shear wall with medium opening. **(d)** Shear wall with large opening.

(Huang 1989) as

$$T = \sum_{i=1}^{N} \frac{1}{2} m_i v_i^2 = \sum_{i=1}^{N} \frac{1}{2} m_i (\omega r_i)^2 = \frac{1}{2}\omega^2 \left[\sum m_i r_i^2\right]; \; I = \sum_{i=1}^{N} m_i r_i^2; \; T = \frac{1}{2} I \omega^2, \quad (36)$$

where in the above expression of kinetic energy, I is the moment of inertia and ω is the angular velocity. The above equation can be comparable in linear terms by replacing the moment of inertia by mass and angular velocity by linear velocity. The Newton's law of rotational motion is given by

$$\tau = I\alpha, \quad (37)$$

where α is the angular acceleration. The lumped mass matrix is purely diagonal and hence computationally cheaper than the consistent mass matrix. Nevertheless, the diagonalization of the mass matrix from the full mass matrix results in the loss of information and accuracy (Huang 1987). There are many ways to lump the mass matrices as described in the literature. Nodal

Table 3 Positive structural responses of shear wall for different opening cases

Damping ζ (%)	No opening			Small opening			Medium opening			Large opening		
	δ (mm)	σ (N/m^2)	τ (N/m^2)	δ (mm)	σ (N/m^2)	τ (N/m^2)	δ (mm)	σ (N/m^2)	τ (N/m^2)	δ (mm)	σ (N/m^2)	τ (N/m^2)
2.5	17.07	6.53	2.38	31.55	15.60	2.96	35.54	2.91	1.73	72.76	7.09	1.83
5.0	13.11	2.06	0.62	23.01	7.23	1.33	27.20	1.61	1.96	35.47	7.60	0.985
7.5	10.79	0.35	0.92	15.00	0.513	0.54	20.90	1.29	0.81	29.50	7.18	1.44
10	10.98	0.66	0.25	10.71	3.28	0.40	19.46	1.70	0.83	87.12	5.59	1.53

Table 4 Negative structural responses of shear wall for different opening cases

Damping ζ (%)	No opening			Small opening			Medium opening			Large opening		
	δ (mm)	σ (N/m^2)	τ (N/m^2)	δ (mm)	σ (N/m^2)	τ (N/m^2)	δ (mm)	σ (N/m^2)	τ (N/m^2)	δ (mm)	σ (N/m^2)	τ (N/m^2)
2.5	38.13	32.50	4.86	41.12	24.1	4.95	45.50	20.10	3.74	275.5	10.70	3.44
5.0	58.20	09.41	1.30	42.14	15.8	3.89	46.13	12.60	3.57	217.4	10.90	3.45
7.5	50.57	14.10	2.25	36.66	24.8	5.01	39.20	12.60	3.00	237.8	09.67	3.27
10	28.24	08.33	1.24	32.56	9.27	2.25	35.25	10.00	2.70	189.1	07.81	3.48

Bending stress (σ) is in 10^7 N/m^2; shear stress (σ) is in 10^6 N/m^2.

quadrature, row sum, and special lumping are the three lumping procedures available to generate the lumped mass matrices. It has found that all three methods of lumping lead to the same mass matrix for nine-node rectangular elements. One of the most efficient means of lumping is to distribute the element mass in proportion to the diagonal terms of consistent mass matrix (Archer and Whalen 2006) and also discarding the off-diagonal elements. This way of lumping has been successfully used in many finite element codes in practice. The advantage of above special lumping scheme is that the assurance of positive definiteness of mass matrix. Lumped

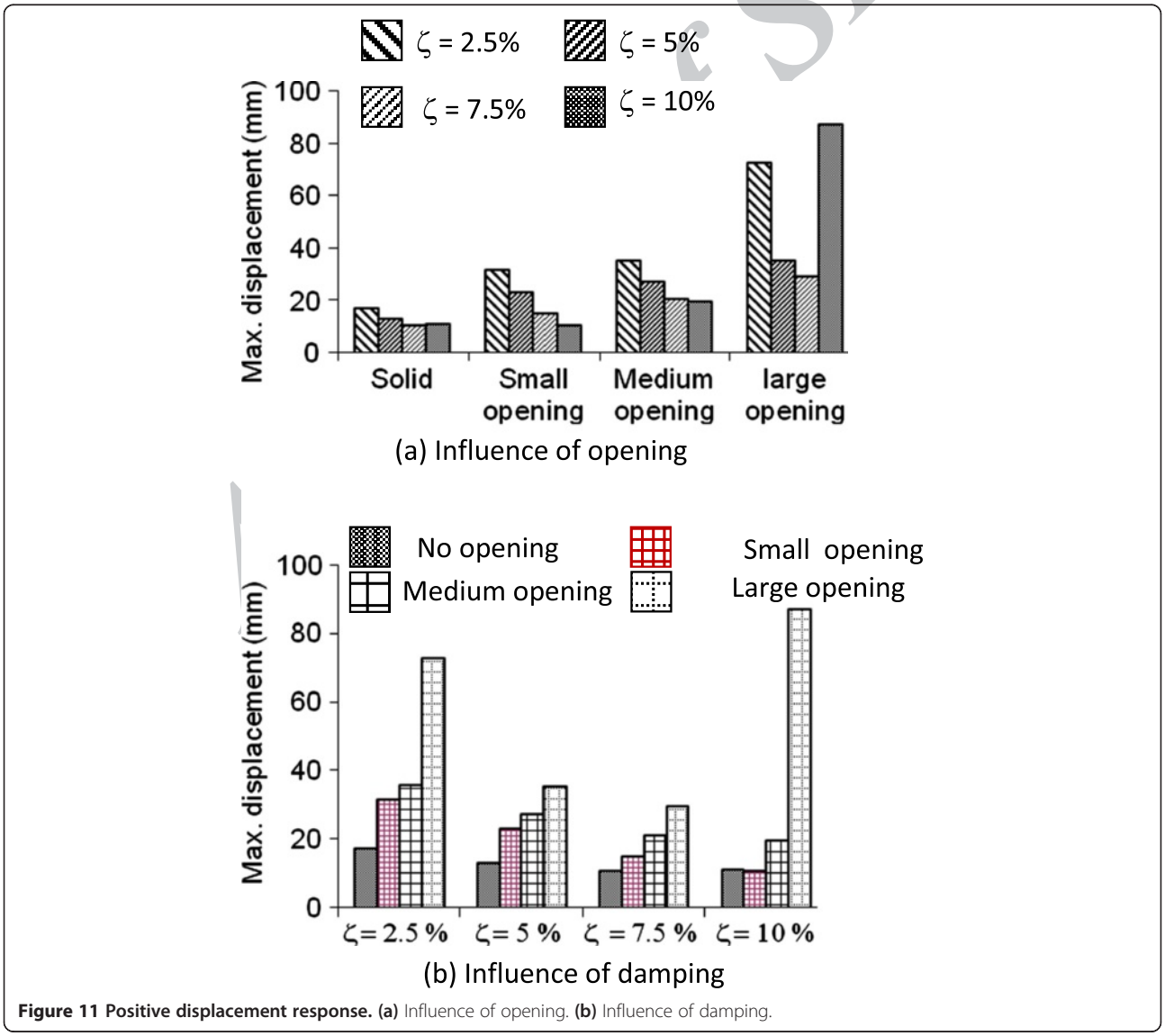

Figure 11 Positive displacement response. (a) Influence of opening. **(b)** Influence of damping.

mass matrix is preferred, if not mandatory, over consistent mass matrix in the case of explicit time integration. The use of lumped mass matrix is mostly employed in lower-order elements. For higher-order elements, the use of lumped mass matrix may not be an appropriate option. Hence, in this study, a consistent mass matrix is employed to formulate the mass matrix.

The linear inertia or translational inertia is given by the following expression:

$$m_{ii} = w_i \int \rho dV. \tag{38}$$

The rotational inertia is given by the following expression:

$$I_{ii} = w_i \int_{V_e} \rho z^{'2} dV = W_i I^{'}$$
$$I^{'} = \int_{V_e} \rho z^{'2} dV, \tag{39}$$

where W_i is the multiplier and ρ is the mass density and z' is the position of the layer with respect to the

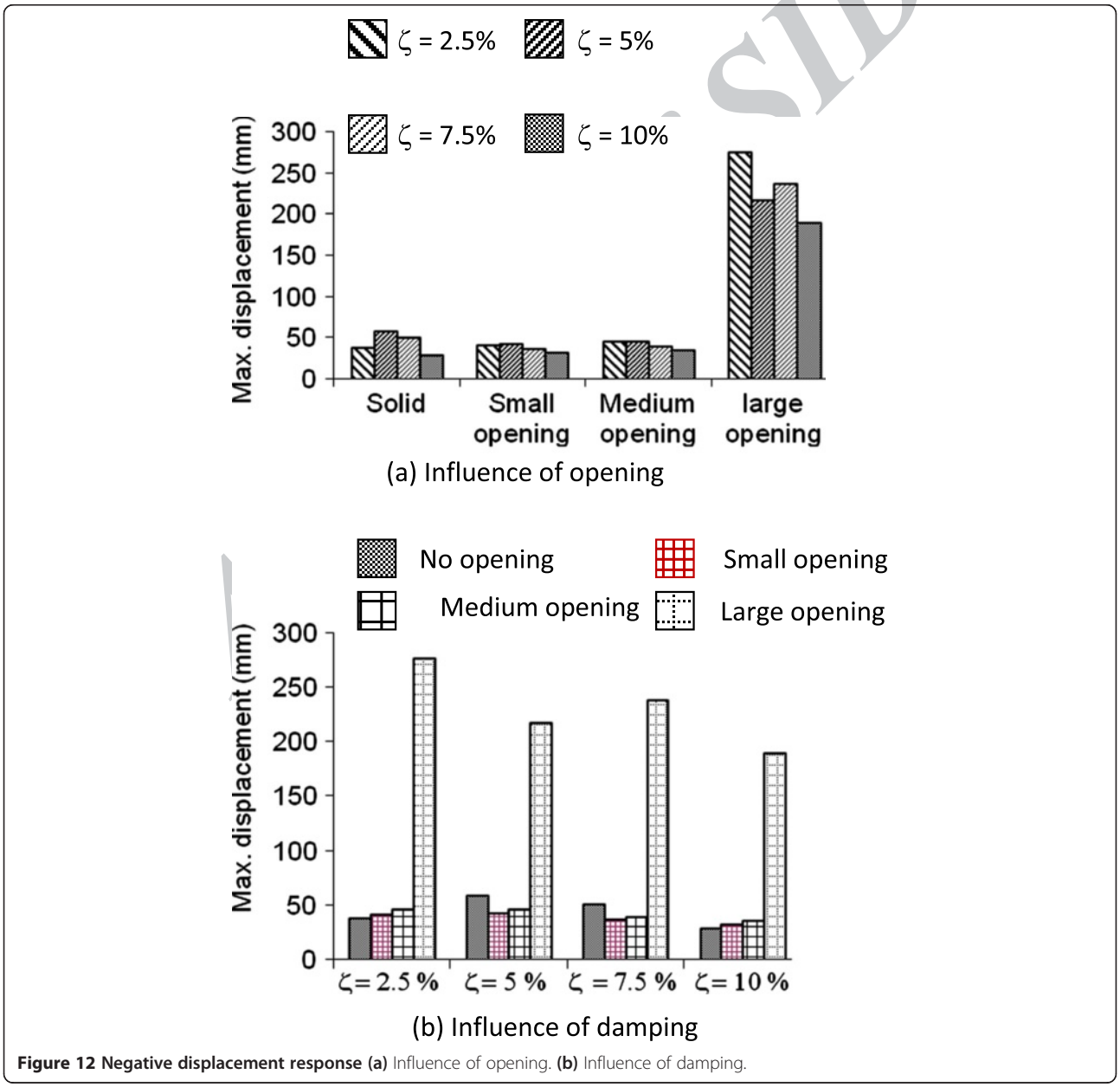

Figure 12 Negative displacement response (a) Influence of opening. **(b)** Influence of damping.

axis of rotation. The multiplier is represented by the following expression:

$$W_i = \frac{\int_{V_e} \rho [N_i][N_i]^T dV}{\sum_{K=1}^{n} \int_{V_e} \rho [N_k][N_k]^T dV}. \quad (40)$$

Formulation of damping matrix

Mass and stiffness matrices can be represented systematically by overall geometry and material characteristics. However, damping can only be represented in a phenomenological manner and thus making the dynamic analysis of structures in a state of uncertainty. Nevertheless, several investigations have been done in making the representation of damping in a simplistic yet logical manner (Zareian and Medina 2010). There is no single universally accepted methodology for representing damping because of the nature of the state variables which control damping. Rayleigh dissipation function assumes that the dissipation of energy takes place and can be idealized as the function of velocity. Damping matrix can be formulated analogous to mass and stiffness matrices (Duggal 2007). When Rayleigh damping is used, the resultant damping matrix is of the same size as stiffness matrix. It is also important to note that the damping matrix should be formulated from damping ratio and not from the member sizes. Rayleigh damping is being used conveniently because of its versatility in segregating each modes independently. The amount of damping can be set appropriately by setting the values of alpha and beta relevantly depending on the requirement of including higher modes.

Sometimes, the additional concentrated damping is also incorporated at selected degrees of freedom in addition to Rayleigh damping. Since damping is a function of velocity, if there is no motion, there will be no damping. It has been

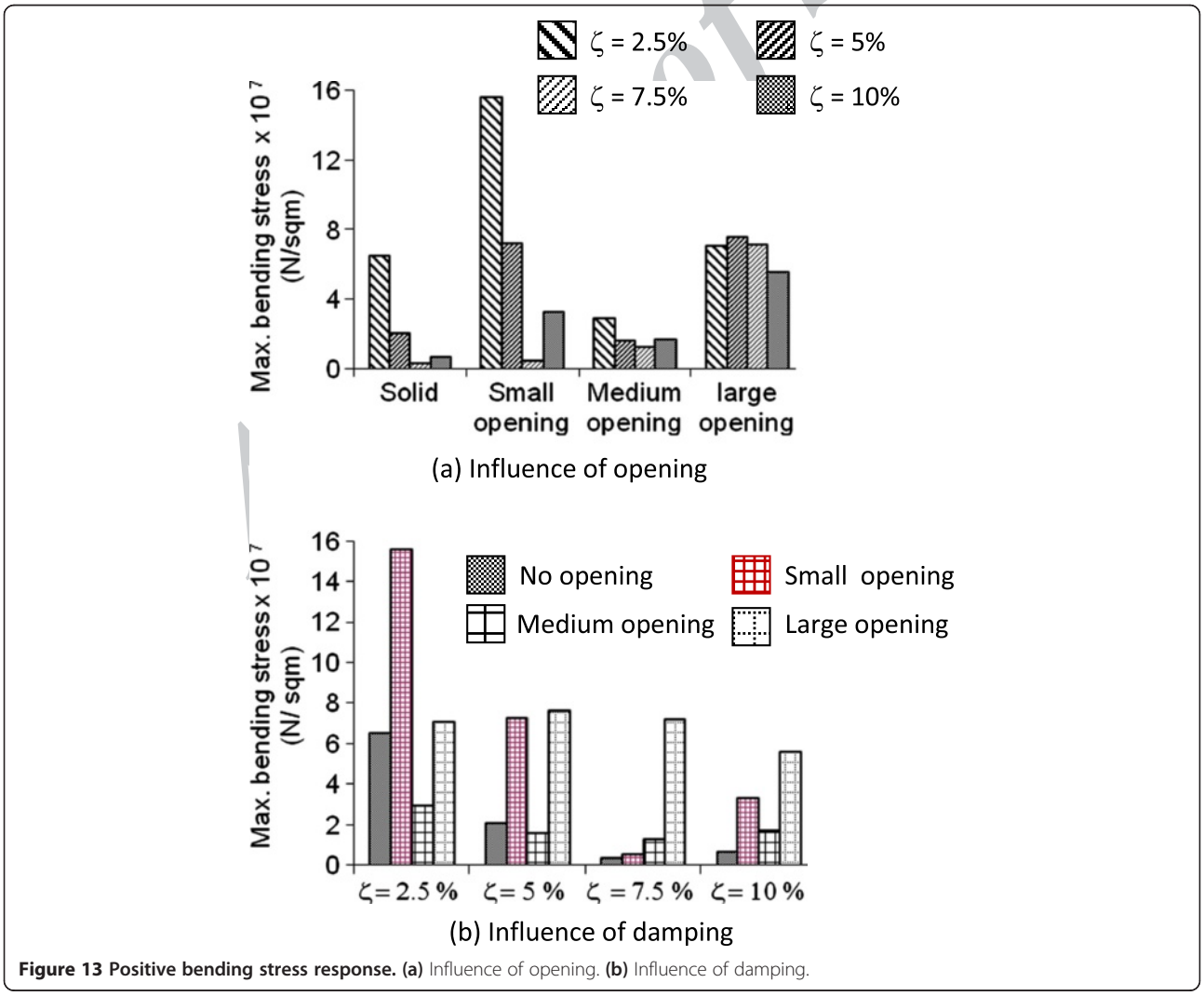

Figure 13 Positive bending stress response. (a) Influence of opening. **(b)** Influence of damping.

mentioned that visco-elastic dampers are being employed in structures to mitigate dynamic effects. Usually, viscous damping is assumed because closed-form solution can be easily available. Very little information is available about variation of damping in linear and nonlinear systems. However, the effect of damping is generally less than the inertial and stiffness effects in most of the practical situations. Therefore, it is reasonable to account for damping by a simplified approximation. The representation of damping through viscous damping coefficient has been in use due to simplicity and accuracy. The damping force is assumed to be proportional to velocity and the constant of proportionality being the viscous damping coefficient. Whenever the system vibrates in a fluid, viscous damping is said to occur. The damping forces are proportional to velocity of the medium and are represented as

$$F = c\dot{u} \tag{41}$$

$$[C] = [M]\sum_{k=0}^{k=p-1}\left(a_k[M]^{-1}[K]\right)^k. \tag{42}$$

In the above equation, $k = 2$ yields

$$[C] = \alpha[M] + \beta[K] \tag{43}$$

$$\zeta_i = \frac{\alpha}{2\omega_i} + \frac{\beta\omega_i}{2}. \tag{44}$$

From the above equation, it is essential to note that if β parameter is 0, the higher modes of the structure will be assigned with very little damping. When the parameter α is 0, the higher modes will be heavily damped as the damping ratio is directly proportional to the frequency (Clough and Penzein 1993). Thus, the choice of damping is problem-dependent. Hence, it is inevitable to perform

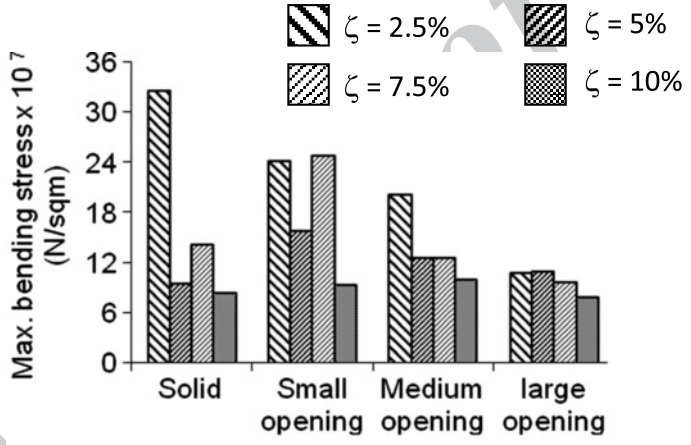

(a) Influence of opening

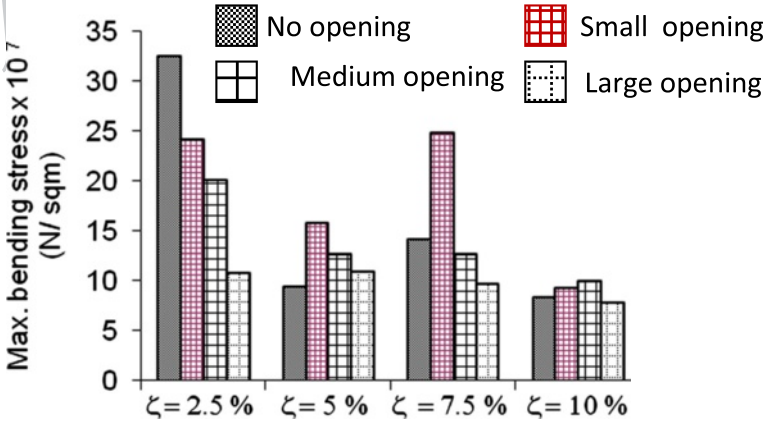

(b) Influence of damping

Figure 14 Negative bending stress response. (a) Influence of opening. **(b)** Influence of damping.

modal analysis to determine the different frequencies for different modes. It is also to be noted that the damping is controlled by only two parameters. Thus, in the Cauchy series, one may include as many terms as possible depending upon the computational efficiency. The use of proportional damping is implemented in most of the finite element codes. The reason for the use of proportional damping is justified by the following explanation. In the equation of motion, the coupling of terms usually occurs which is reflected in the mass and stiffness matrices. Inertia coupling is present when the mass matrix is non-diagonal, and static coupling is present when the stiffness matrix is non-diagonal. The coupling of the modes usually can be avoided easily in the case of undamped free vibration, but the same is not true for damped vibration. Hence, in order to represent the equation of motion in uncoupled form, it is suggested to have a damping matrix proportional to the uncoupled mass and stiffness matrices. Thus, Rayleigh's proportional damping has the specific advantage in the sense that the equation of motion can be uncoupled when it is proportional to mass and stiffness matrices. Thus, it is proposed to use Rayleigh damping in this study.

Nonlinear solution

The numerical procedure for nonlinear analysis employs the iterative procedure to satisfy the equilibrium at the end of the load step. Once the convergence of the solution is achieved, the algorithm proceeds to the next step. It is always desirable to keep the load step very small especially after the onset of nonlinear behavior. The stiffness matrix is updated at the beginning of each load step. The convergence is said

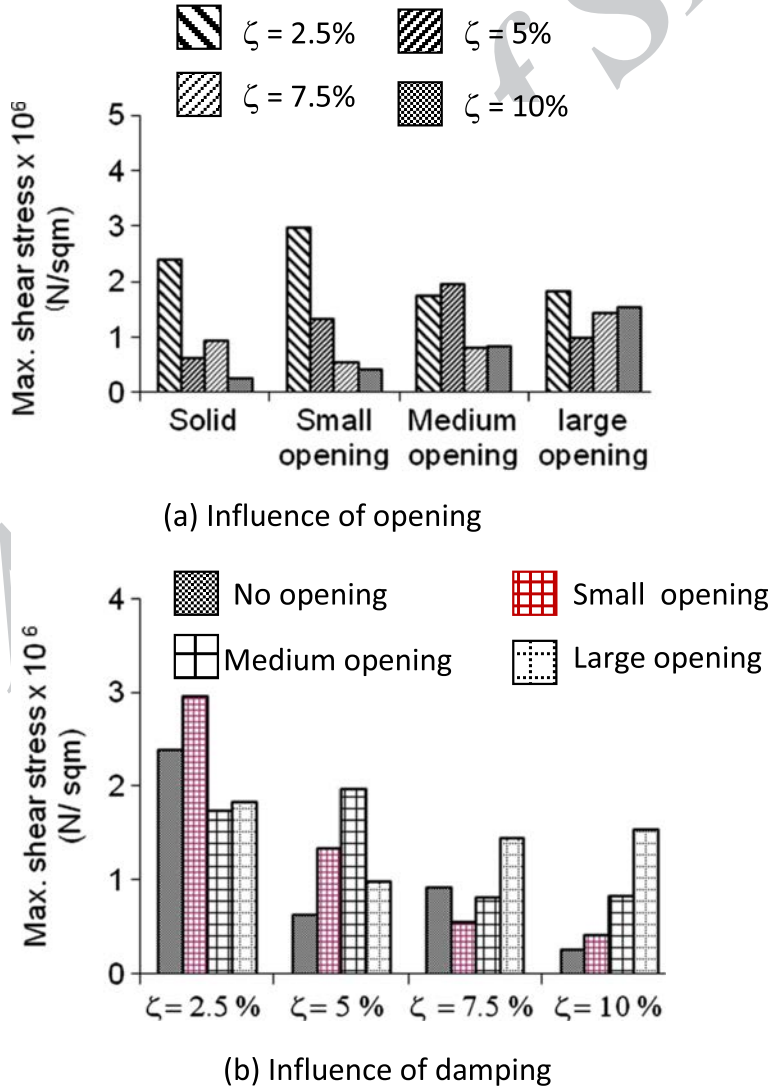

Figure 15 Positive shear stress response. (a) Influence of opening. **(b)** Influence of damping.

to be achieved if the out-of-balance forces, calculated as under, is less than the specified tolerance:

$$\psi_i^n = f^n - p_i^n = f^n - \int_V B^T \sigma_i^n \, dV \quad < \text{tolerance } (0.0025). \quad (45)$$

Results and discussion

A reinforced concrete squat square shear wall, 3.6 m × 3.6 m with 0.2-m thick, subjected to EL Centro earthquake loading over the period of 31.18 s with a peak ground acceleration of +0.29 g, as shown in Figure 6, has been considered. For the finite element dynamic analysis, the entire shear wall is discretized using the nine-node degenerated shell elements of size (0.6 m × 1.2 m). The discretizations of the shear wall for solid and opening cases are shown in Figure 7. The displacement response has been calculated for a period of 40 s for different damping ratios 2.5%, 5%, 7.5%, and 10%, using Newmark β method with constant acceleration scheme. In order to investigate the size of opening on structural behavior of shear wall, the results of shear wall with no opening are compared with shear wall with three different sizes of openings, namely, (a) small opening (1.2 m × 1.2 m), (b) medium opening (1.2 m × 2.4 m), and (c) large opening (2.4 m × 2.4 m).

For the finite element analysis, the Young's modulus of elasticity of the concrete is taken as 2.98×10^{10} N/m^2 and Poisson's ratio is taken as 0.17. The undeformed and deformed shapes of the shear walls with and without openings are shown in Figure 7. The displacement and stresses (bending and shear) are grouped into positive (if the value is above the horizontal axis of the time history)

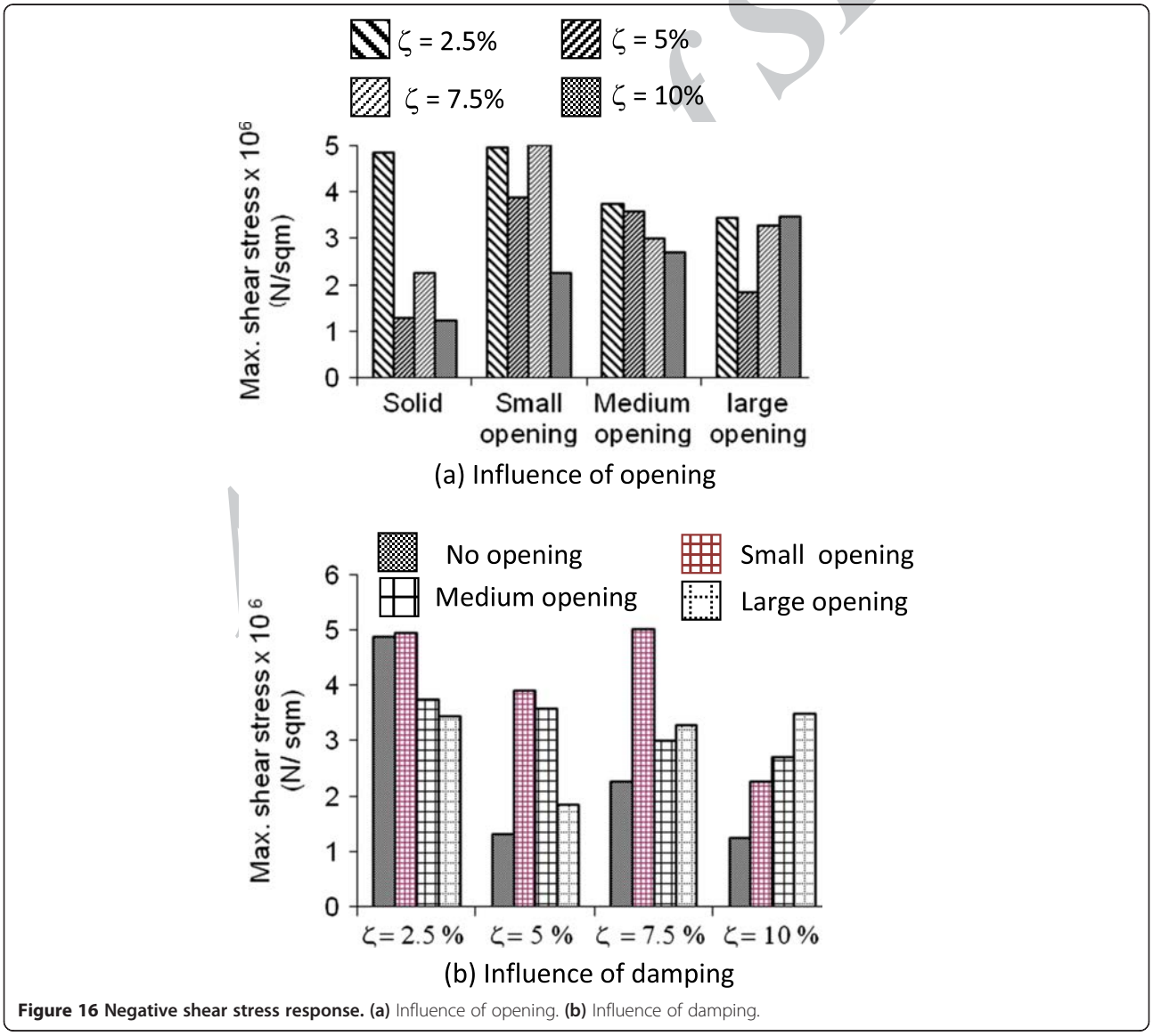

Figure 16 Negative shear stress response. (a) Influence of opening. **(b)** Influence of damping.

and negative (if the value is below the horizontal axis of the time history), and, accordingly, the graphs and tables are also presented in this study. The deformed shapes (positive and negative deformations) of solid shear wall and shear wall with small, medium, and large openings are qualitatively plotted in Figure 7 in order to highlight the mode in which the shear wall deforms. The mode of deformation of solid shear wall and shear wall with small opening is almost similar. On the other hand, shear wall with medium and large openings characterizes the shear mode of deformation. Hence, it is concluded that the racking deformation becomes important in the presence of medium- as well as large-sized openings. The displacement, bending stress, and shear stress time-history responses for various opening sizes, *viz.*, no opening, small opening, medium opening, and large opening with damping ratios $\zeta = 2.5\%$, 5%, 7.5%, and 10% are plotted in Figures 8,9,10, respectively.

It is obvious from Figure 8 that the increase in the opening size of shear wall has the strong influence on the displacement response, which is measured at the top of the shear wall, as evident from various time histories as well from Tables 3 and 4. From Figure 8, it was observed that shear wall with large opening resulted in huge displacement and the influence of damping has not been found to be substantially benefitting in controlling the response. Moreover, as can be seen in Figure 8, displacements were predominantly on the negative side (referred in this study as negative displacement) and thus indicate that the structure is behaving in the one-sided cyclic fashion characterizing the instability of the structure. The negative displacement values (as observed from Table 4) also validate the same. Hence, it is advisable to avoid large openings in the shear wall for better structural response (Figures 11 and 12). On the other hand, increase in damping has a significant effect on the structural response.

The bending stress responses measured at the bottom of the shear wall for various opening cases are plotted in Figure 9. It was observed that the bending stresses of shear wall with no openings, small opening, and medium opening almost follow the same trend with not much reversal of stresses which are on the negative side. However, in the case of large opening, the huge reversal of stresses taking over the entire time history indicates that the structure is heavily stressed and such openings are to be avoided in practice. As expected, damping has not resulted in substantial mitigation of the structural damage for shear wall with large openings (Figures 13 and 14).

The shear stress responses of shear wall measured at the bottom of the shear wall for various opening cases are plotted in Figure 10. The response history of shear stress for shear wall with various opening cases indicates that for large openings, the shear stresses are found to be affected by damping ratios to the great extent. Shear stresses were found to be minimal for shear wall with no opening, and damping has a pronounced effect on the shear wall with no opening and with small opening cases (Figures 15 and 16). Since only proportional stiffness damping was used throughout the study, higher modes were considerably damped and hence, the responses (displacement and stresses) decayed toward the end of the time step to a greater extent.

Conclusions

In this paper, the influence of opening sizes on the structural response of squat square shear wall, 3.6 m × 3.6 m and 0.2 m thick subjected to EL Centro earthquake loading and applied over the period of 31.18 s, has been investigated for different damping ratios (2.5%, 5%, 7.5%, and 10%) using nonlinear finite element analysis. In addition, the following conclusions have been drawn:

1. Racking deformation becomes paramount for shear walls with medium and large openings.
2. The shear wall with large openings is to be avoided as it results in instability with one-sided cyclic behavior.
3. Higher modes have been considerably damped due to the presence of stiffness proportional damping.

Competing interests
Both authors declare that they have no competing interests.

Authors' contributions
Both authors read and approved the final manuscript.

Authors' information
G. Muthukumar is a Lecturer in the Department of Civil Engineering, BITS Pilani. Prof. Manoj Kumar is an Associate Professor & Head in the Department of Civil Engineering, BITS Pilani.

Received: 14 December 2012 Accepted: 25 July 2013
Published: 11 Nov 2013

References

Ahmad S, Irons BM, Zienkiewicz OC (1970) Analysis of thick and thin shell structures by curved finite elements. Int J Numerical Methods Eng 2:419–451
Archer GC, Whalen TM (2006) Development of rotationally consistent diagonal mass matrices for plate and beam elements. Comput Methods Appl Eng 194:675–689
Baratta A, Corbi O (2010) An approach to masonry structural analysis by the no-tension assumption—part 1: material modeling, theoretical setup, and closed form solutions. ASME Appl Mech Rev 63:1–17
Baratta A, Corbi O (2012) FRP composites retrofitting for protection of monumental and ancient constructions. The Open Construction and Building Technology Journal 6:361–367
Baratta A, Corbi I, Corbi O (2008) Stress analysis of masonry structures: arches, walls and vaults, structural analysis of historic construction: preserving safety and significance. Proceedings of the 6th international conference on structural analysis of historic construction, SAHC08 1:321–329
Baratta A, Corbi I, Corbi O, Barros RC, Bairrao R (2012) Shaking table experimental researches aimed at the protection of structures to dynamic loading. The Open Construction and Building Technology Journal 6:355–360

Baratta A, Corbi I, Corbi O, Barros RC, Bairrao R (2013) Towards a seismic worst scenario approach for rocking systems: analytical and experimental set-up for dynamic response. Acta Mechanica 224:691–705
Bathe KJ (2006) Finite element procedures. Prentice Hall of India Private Limited, New Delhi
Cedolin L, Crutzen YRJ, Deipoli (1977) Triaxial stress-strain relationships for concrete. ASCE Journal of the Engineering Mechanics Division 103:423–439
Chen WF (1982) Plasticity in reinforced concrete. McGraw-Hill, New York
Clough RW, Penzein J (1993) Dynamics of structures. McGraw Hill, New York
Collins MP, Mitchell D (1980) Shear and torsion design of prestressed and non-prestressed concrete beams. J PCI 25:32–100
Corbi I (2013) FRP reinforcement of masonry panels by means of C-fiber strips. Composites Part B: Engineering 47:348–356
Derecho AT, Ghosh SK, Iqbal Q, Fintel M (1979) Strength, stiffness, and ductility required in reinforced concrete structural walls for earthquake resistance. ACI Struct J 76:875–896
Duggal SK (2007) Earthquake resistant design of structures. Oxford Higher Education, Oxford University Press, New Delhi
Gasparani G, Trombetti T, Silvestri S, Ricci I, Ivorra Chorro S, Foti D (2013) Preliminary results of a shaking table tests on a 3-storey building realized with cast in place sandwich squat concrete walls. In: modern methods and advances in structural engineering and construction: the seventh international structural engineering and construction conference (ISEC-7). , Honolulu, Hawaii
Huang (1987) Implementation of assumed strain degenerated shell elements. Comput Struct 25:147–155
Huang HC (1989) Static and dynamic analyses of plates and shells: theory, software and applications. Springer, London
Kant T, Kumar S, Singh UP (1994) Shell dynamics with three-dimensional degenerate finite elements. Comput Struct 50:135–146
Kim HS, Lee DG (2008) Analysis of shear wall with openings using super elements. Eng Struct 25:981–991
Kuang JS, Ho YB (2008) Seismic behavior and ductility of squat reinforced concrete shear walls with nonseismic detailing. ACI Struct J 105:225–231
Lefas ID, Kosovos MD, Ambraseys NN (1990) Behavior of reinforced concrete structural walls, strength, deformation characteristics, and failure mechanism. ACI Struct J 87:23–31
Liu Y, Teng S (2008) Nonlinear analysis of reinforced concrete slabs using non-layered shell element. ASCE, J Struct Eng 134:1092–1100
MacLeod IA (1970) Shear wall-frame interaction- a design aid. Engineering Bulletin, Portland Cement Association (PCA)
Mo YL (1988) Analysis and design of low-rise structural walls under dynamically applied shear forces. ACI Struct J 85:180–189
Mullapudi RT, Charkhchi P, Ayoub AS (2009) Evaluation of behavior of reinforced concrete shear walls through finite element analysis. ACI Special Publication 265:73–100
Nayal R, Rasheed HA (2006) Tension stiffening model for concrete beams reinforced with steel and FRP Bars. ASCE, J Mater 146:831–841
Neuenhofer A (2006) Lateral stiffness of shear walls with openings. ASCE, J Struct Eng 132:1846–1851
Ngo D, Scordelis AC (1967) Finite element analysis of reinforced concrete beams. ACI Struct J 64:152–163
Owen DRG, Hinton E (1980) Finite elements in plasticity. Theory and practice, Pineridge Press Limited, UK
Paknahad M, Noorzaei J, Jaafar MS, Thanoon WA (2007) Analysis of shear wall structure using optimal membrane triangle element. Finite Element in Analysis and Design 43:861–869
Paswey SF, Clough RW (1971) Improved numerical integration of thick shell finite elements. Int J Numerical Methods Eng 3:575–586
Rahimian A (2011) Lateral stiffness of concrete shear walls for tall buildings. ACI Struct J 108:755–765
Rashid YR (1968) Analysis of prestressed concrete pressure vessels. Nuclear Engineering Design 7:334–344
Ricci I, Gasparini G, Silvestri S, Trombetti T, Foti D, Ivorra Chooro S, Ivorra Chooro S (2012) Design of a shaking table test on a 3-storey building composed of cast-in-situ concrete walls. Proceedings of the 15th World Conference on Earthquake Engineering (15WCEE), Lisbon
Rosman R (1964) Approximate analysis of shear walls subjected to lateral loads. ACI Journal 64:717–734
Schwaighofer J (1967) Door openings in shear walls. ACI Journal 64:730–734
Taylor CP, Cote PA, Wallace JW (1988) Design of sender reinforced concrete walls with openings. ACI Struct J 95:420–433
Teng S, Liu Y, Soh CK (2005) Analysis of concrete slabs using shell element with assumed strain. ACI Struct J 102:515–524
Vecchio FJ, Collins MP (1986) The modified compression field theory for reinforced concrete elements subjected to shear. ACI Journal 83:219–231
Willam K, and Warnke E (1975) Constitutive model for triaxial behavior of concrete. Proceedings of the International Association for Bridge and Structural Engineering, 19 Zurich, Switzerland 1-30.
Zareian F, Medina RA (2010) A practical method for proper modeling of structural damping in inelastic plane structural systems. Comput Struct 88:45–53
Zienkiewicz OC, Taylor RL, Too JM (1971) Reduced integration techniques in general analysis of plates and shells. Int J Numerical Methods Eng 3:575–586

10.1186/2008-6695-5-27
Cite this article as: Gopalarathnam and Kumar: **Nonlinear finite element dynamic analysis of squat shear wall with openings.** *International Journal of Advanced Structural Engineering* 2013, 5:27